

Anisotropic elasticity of IVB transition-metal mononitrides determined by *ab initio* calculations

Shijo Nagao*

Nordic Hysitron Laboratory, Department of Materials Science and Engineering, Helsinki University of Technology, P. O. Box 6200, 02015 HUT, Finland

K. Nordlund

Accelerator Laboratory, University of Helsinki, P. O. Box 43, FIN-00014, Finland

R. Nowak

Nordic Hysitron Laboratory, Department of Materials Science and Engineering, Helsinki University of Technology, P. O. Box 6200, 02015 HUT, Finland

(Received 10 February 2006; published 27 April 2006)

Elastic parameters of IVB transition-metal mononitrides, TiN, ZrN, and HfN in the cubic NaCl crystal structure have been calculated by means of density-functional theory with the generalized gradient approximation. The elastic constants c_{11} , c_{12} , and c_{44} were shown to be sufficiently converged with the density of the \mathbf{k} -point mesh in the deformed Brillouin zone to discuss the elastic anisotropy of the systems. It was found that the anisotropy coefficient $\kappa \equiv (c_{11} - c_{12})/2c_{44}$ increases with the atomic number of the metal element, i.e., HfN exhibits as strong anisotropy as $\kappa = 2.02$. The Young's modulus of HfN along $\langle 100 \rangle$ is approximately two times higher than that along $\langle 111 \rangle$. Moreover, analysis of the deformation energy by the applied strain modes shows that this elastic anisotropy originates from the strong covalent bonding between metal and nitrogen atoms along $\langle 100 \rangle$.

DOI: [10.1103/PhysRevB.73.144113](https://doi.org/10.1103/PhysRevB.73.144113)

PACS number(s): 62.20.Dc, 81.40.Jj, 46.25.-y, 81.05.Je

I. INTRODUCTION

The transition metal nitrides have attracted considerable attention during the past three decades due to their interesting combination of mechanical, electrical, and chemical properties. This has led to their wide application as hard coatings and thin films for electronic devices (for a review, see Ref. 1). In particular, their high activation energy against electromigration, coupled with superior electrical conductivity, high melting point, and excellent chemical stability has made these "refractory hard metals" extensively used for diffusion/reaction barriers in metallization schemes for semiconductor and photovoltaic technology, and desirable candidates for new materials in electronic devices.²⁻⁵ Furthermore, the discovery of ZrN and HfN-based new layer-structured high T_c superconductors,⁶⁻⁸ as well as the recent synthesis of superconducting nitrides with a new structure (Zr_3N_4 and Hf_3N_4)⁹ has attracted much attention to these materials. However, the main interest in transition metal nitrides is associated with their superior mechanical properties, partially related to electronic structure,¹⁰ that are usually tailored by the selection of specific deposition conditions,^{11,12} or modified by post-growth ion treatment.¹³⁻¹⁵

Surprisingly enough, despite common reference to the "extreme hardness" and "significant Young's modulus" of transition metal nitrides, there is considerable confusion regarding what the acceptable values of the mechanical characteristics are. Various authors have reported inconsistent results for HfN thin films, that are relatively rarely examined, as well as for widely investigated TiN and ZrN. Indeed, the discrepancy in HfN hardness measured by various authors spans from 16 to 60 GPa,¹⁶⁻²¹ which made Nowak *et al.*²² question the appropriateness of indentation tests in the case

of nitride hard films on silicon substrates. Moreover, a recent *ab initio* calculation work by Zhang and He²³ alerted that two "widely accepted," but considerably different values of the Young's modulus for TiN are nowadays in common use, namely, 250 and 640 GPa.

The above evidence raises serious reservations towards results of the majority of the research that is related to the mechanical properties of the metal nitride films. The extensive documentation of ultrahigh internal stresses that are generated in TiN, ZrN, and HfN during deposition serves as an example of a field that would be much affected by drastic correction of the accepted values, since the methods of stress evaluation employ equations that inevitably require accurate knowledge of elastic parameters for both the film and substrate.^{13-15,24,25} Furthermore, there is still uncertainty concerning the origin and scale of the anisotropic lattice distortion and related elastic anisotropy exhibited by the transition of metal nitride films²⁶ that was never addressed in a systematic manner so far.

Hence, the present paper provides a thorough study of the elastic anisotropy of HfN, ZrN, and TiN, by employing advanced *ab initio* calculations, which frequently start with the determination of electronic structure using density-functional theory (DFT) within the local density approximation (LDA) and generalized gradient approximation (GGA).²⁷ In contrast to the few previously reported *ab initio* calculations of elastic constants of hard refractory metals with pseudopotentials^{21,28} or the full-potential augmented plane wave method (FLAPW),²⁹ which used a fixed density wave vector \mathbf{k} -point mesh within the Brillouin zone, the current work presents a methodical mesh-dependent convergence analysis of the results. The first explanation of the nature of the elastic anisotropy is offered, enabling distinguishing the elastic aniso-

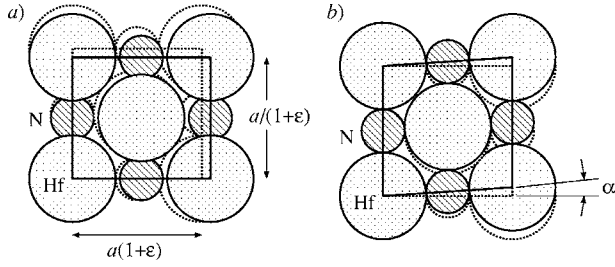


FIG. 1. Schematic drawing of the two-dimensional deformation modes applied to the HfN crystal with lattice constant a . Orthorhombic deformation (a) is denoted by the strain ε , and simple shear deformation (b) by $\gamma = \tan \alpha$.

tropy of HfN with respect to ZrN and TiN. The theoretically evaluated anisotropy of the Young's modulus for TiN, ZrN, and HfN appears to be in agreement with the only available literature values obtained from x-ray diffraction experiments by Perry.³⁰

The additional motivation of our calculations is to obtain the parameters that are necessary to construct the analytical interatomic potentials for HfN, which in turn should allow us to carry out molecular dynamics simulations of phenomena involving large numbers of atoms such as nanoindentation surface deformation or ion irradiation effects.^{31–35}

II. COMPUTATIONAL DETAILS

The present DFT calculations on the IVB metal nitrides have been carried out by employing the ESPRESSO/PWSCF software package.³⁶ We use Vanderbilt ultrasoft pseudopotentials³⁷ with GGA, where a scalar-relativistic calculation is applied for the transition metal elements, and a nonrelativistic one for nitrogen. These pseudopotentials have been confirmed to give proper electronic band structure and density of states (DoS) for the cubic NaCl structure for the nitrides, similar to those obtained by FLAPW.²⁹ Each self-consistent field calculation is converged to give high accuracy of the total energy within 1.0×10^{-9} Ry. The kinematical cutoff energy of the wave function is selected to be 80 Ry, as higher cutoff energy of 100 and 120 Ry have been found not to change the results.

The stress theory of Nielsen and Martin³⁸ enables us to calculate the stress tensor σ_{ij} of a given crystal structure from a self-consistent field obtained by DFT. By this theory, the equilibrium lattice constant a_0 can be linearly interpolated at the pressure $P=0$ in between different lattice constants, while the bulk modulus is given by

$$B = - \left. \frac{a_0}{3} \frac{dP}{da} \right|_{a=a_0}, \quad (1)$$

for a cubic system. To obtain the independent elastic constants of a cubic system, namely c_{11} , c_{12} , and c_{44} in Voigt notation, we apply volume-conserving homogeneous deformations on the equilibrium unit cell (see Fig. 1). The strain tensor u_{ij} of the orthorhombic deformation is denoted by a single strain parameter ε as

$$\{u_{ij}\} = \begin{pmatrix} \varepsilon & 0 & 0 \\ 0 & -\varepsilon/(1+\varepsilon) & 0 \\ 0 & 0 & 0 \end{pmatrix}, \quad (2)$$

and that of the shear deformation by γ as

$$\{u_{ij}\} = \begin{pmatrix} 0 & \gamma/2 & 0 \\ \gamma/2 & 0 & 0 \\ 0 & 0 & 0 \end{pmatrix}. \quad (3)$$

Under the condition $\varepsilon, \gamma \ll 1$, Hooke's law gives

$$c_{11} - c_{12} = (\sigma_1 - \sigma_2) \left(\varepsilon + \frac{\varepsilon}{1+\varepsilon} \right)^{-1}, \quad (4)$$

$$c_{44} = \sigma_4 / \gamma, \quad (5)$$

also in Voigt notation. Since the bulk modulus is related to the elastic constants as

$$B = \frac{1}{3}(c_{11} + 2c_{12}), \quad (6)$$

we consequently obtain the elastic constants

$$c_{11} = B + \frac{2}{3}(c_{11} - c_{12}), \quad (7)$$

$$c_{12} = B - \frac{1}{3}(c_{11} - c_{12}), \quad (8)$$

using B from Eq. (1).

Here the smallest strain $\gamma = \varepsilon = 0.002$ that assures sufficient numerical accuracy of the calculated pressure, i.e., of the elastic constants, is selected.

Since the materials are metallic, special care should be taken about electrons in the vicinity of the Fermi energy. The first order Methfessel-Paxton smearing function applied here is known to give rapid but not monotonic convergence of the integration over the Brillouin zone with an increasing number of sampling \mathbf{k} points.³⁹ The broadening energy of the smearing is selected to 10 mRy for accurate calculations. To assure the convergence of elastic constants calculations, a series of self-consistent field calculations are achieved for various densities of \mathbf{k} points, where the standard Monkhorst-Pack method⁴⁰ is applied to generate a homogeneous \mathbf{k} -point mesh in the irreducible Brillouin zone of each deformed unit cell. Figure 2 shows the convergence of physical parameter calculations such as the total energy, lattice constant, bulk modulus, and elastic constants ($c_{11}-c_{12}$) and c_{44} calculated with the wide range of the number of \mathbf{k} points from 29 up to 6992, which correspond to a $8 \times 8 \times 8$ mesh in the irreducible Brillouin zone of the cubic structure and a $30 \times 30 \times 30$ mesh in the one under shear strain. Due to the high symmetry of the cubic structure preserved for the homogeneous expansion, the convergence of the bulk modulus and lattice constant is rapid enough to give meaningful values within the possible numerical errors at the smallest number of \mathbf{k} points. In contrast, the elastic constants require a denser \mathbf{k} -point mesh to converge within an error of a few percent; at least 1500 and 4000 \mathbf{k} points for c_{44} and ($c_{11}-c_{12}$), respec-

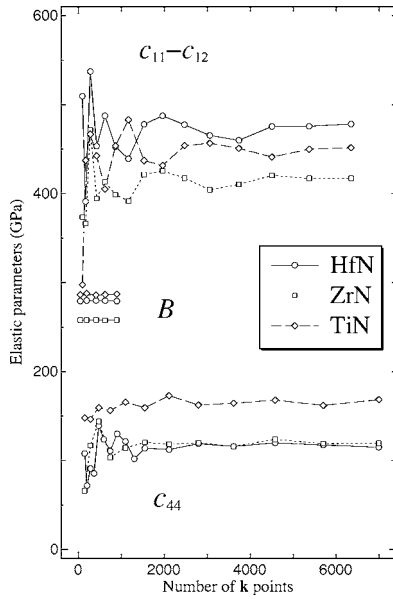


FIG. 2. Convergence of elastic parameters with increasing sampling \mathbf{k} points in the irreducible Brillouin zone.

tively. The total energies of the deformed unit cells corresponding to these elastic constants remains within about 1 mRy for the whole range of the number of \mathbf{k} points, and converged to less than 0.1 mRy for accurate elastic constant calculations.

Note that both of these elastic constants are robust against the shift of the equilibrium cell size under zero pressure. Such a shift happens when the \mathbf{k} mesh is changed, and induces some amount of hydrostatic pressure. For shear defor-

mation, Eq. (5) uses only a nondiagonal component of the stress tensor that never appears at the equilibrium point. Orthorhombic deformation activates the diagonal components of the stress, but the effect of hydrostatic pressure is canceled out in Eq. (4). Thus the elastic constants calculations are not affected by the shift during the \mathbf{k} convergence test.

III. RESULTS AND DISCUSSION

The calculated elastic constants are listed in Table I together with the values available in the recent literature. Errors of the results are estimated from the standard deviations of several data toward \mathbf{k} convergence. The present lattice constants and bulk moduli show good agreement with those from other calculations, in particular, those obtained with GGA. However, the elastic constants obtained in the present calculations tend to show smaller values than those in the literature. The likely reason to this discrepancy is the density of sampling \mathbf{k} points in the Brillouin zone. The \mathbf{k} point meshes in the references are less dense than the density that gives convergence of elastic constants in the present study.

Based on the obtained elastic constants, the anisotropic Young's modulus E can be examined for the materials. If we describe the crystallographic direction represented by

$$\Gamma = \frac{h^2k^2 + k^2l^2 + l^2h^2}{(h^2 + k^2 + l^2)^2}, \quad (9)$$

we can write E of a cubic system as a function of Γ :

TABLE I. Equilibrium lattice constant a_0 (Å), bulk modulus B , elastic constants c_{11} , c_{12} , and c_{44} (GPa) of HfN, ZrN, and TiN in the NaCl structure. Errors in the table are estimated from the standard deviations of several data toward \mathbf{k} convergence. Other figures by recent GGA and LDA studies are listed for comparison.

System	Method		a_0	B	c_{11}	c_{12}	c_{44}
HfN	Present work	GGA	4.539	279.8(2)	597(1)	121(1)	118(2)
		APW+lo ^a	LDA	4.53	284	733	124
	FLAPW ^b	GGA			664	115	154
		LDA	4.37	320			
		GGA	4.54	278			
ABINIT ^c	LDA		306	694	112	134	
ZrN	Present work	GGA	4.593	257.9(1)	537(1)	118(1)	120(3)
		FLAPW ^b	GGA	4.57	264		
	LDA	4.53	292				
		ABINIT ^c	LDA		285	611	117
TiN	Present work	GGA	4.246	286.6(5)	585(4)	137(2)	165(3)
		APW+lo ^a	GGA			598	154
	FLAPW ^b	LDA	4.18	318	669	160	215
		GGA	4.26	286			
		LDA	4.18	322			

^aReference 28, with $4 \times 4 \times 4$ \mathbf{k} -point mesh.

^bReference 29, with $8 \times 8 \times 8$ \mathbf{k} -point mesh.

^cReference 21, with $16 \times 16 \times 16$ \mathbf{k} -point mesh.

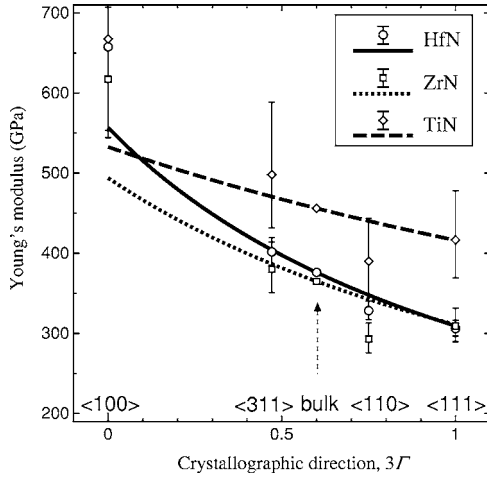


FIG. 3. Anisotropic Young's moduli E derived from the calculated elastic constants of HfN, ZrN, and TiN. The data in Ref. 30 are rescaled at $3\Gamma=0.6$ and plotted with error bars that are given by the assumption that the intercept lattice constants have an uncertainty of 0.002 \AA .

$$E = \left[s_{11} - 2 \left(s_{11} - s_{12} - \frac{1}{2} s_{44} \right) \Gamma \right]^{-1}, \quad (10)$$

where the components of the compliance tensor s_{11} , s_{12} , and s_{44} are derived from the elastic constants by a standard procedure.⁴¹ This function is plotted for HfN, ZrN, and TiN in Fig. 3, and the values of E at some special Γ are listed in Table II, namely $E_{\langle 100 \rangle}$ at $3\Gamma=0$, $E_{\langle 111 \rangle}$ at $3\Gamma=1$, and E_{bulk} at $3\Gamma=0.6$. The latter value is accepted for bulk polycrystalline materials (see the note added in Ref. 30). Also, the anisotropy coefficients $\kappa \equiv (c_{11} - c_{12})/2c_{44}$ are shown for the systems in the same table. It is obvious that HfN has strong anisotropy in the elasticity as $\kappa > 2$; $E_{\langle 100 \rangle}$ is almost two times higher than $E_{\langle 111 \rangle}$. On the contrary, TiN behaves close to isotropic materials, despite of the cubic symmetry of the NaCl crystal structure.

For comparison with the x-ray diffraction (XRD) experiments by Perry,³⁰ the intercept lattice constants a_{hkl} in the article are converted into anisotropic Young's modulus as follows:

$$E_{hkl} = E_{\text{bulk}} \frac{a_{\text{bulk}} - a_0}{a_{hkl} - a_0}. \quad (11)$$

The values of a_0 and a_{bulk} are as they appeared in his paper, while the Young's modulus for bulk polycrystalline materials E_{bulk} , which is taken from the literature, is replaced with our

TABLE II. Anisotropic Young's moduli and anisotropy coefficients $\kappa \equiv (c_{11} - c_{12})/2c_{44}$ of HfN, ZrN and TiN.

System	E_{bulk}	$E_{\langle 100 \rangle}$	$E_{\langle 111 \rangle}$	κ
HfN	376	557	309	2.02
ZrN	365	494	311	1.75
TiN	456	533	416	1.36

TABLE III. Deviation of the bond lengths and angle of metal mononitrides in the NaCl crystal structure with the orthorhombic and shear strain. See Fig. 1 for the definition of the strains represented by ε and γ .

Mode	$\Delta L_{M-N}/L_{M-N}$	$\Delta L_{M-M}/L_{M-M}$	$\Delta \theta_{M-M-N}$
Ortho.	$\pm \varepsilon$	ε^2	ε
Shear	$\gamma^2/2$	$\pm \gamma^2/2$	$\gamma/2$

calculated values. The obtained E_{hkl} are also plotted in Fig. 3, where the error bars are drawn only for the current discussion by assuming the intercept lattice constants have an uncertainty of 0.002 \AA . Even though these experimental values may be affected by the textured structure in the thin films, the measured anisotropy follows the calculated Young's modulus. This is one evidence that the macroscopic elasticity of these hard materials is mainly controlled by the original property of crystals, not by microstructures in each specimen.

To figure out the origin of the anisotropy variation among these material systems, one has to consider the relationship between the deformation energy and the changes of bonding geometry in the NaCl crystal structure. The bond length L_{M-M} , L_{M-N} and the angle θ_{M-M-N} in the deformed crystal can approximately be written by the strain parameters $\gamma/2$ and ε (see Table III). Here M represents a metal element and N nitrogen. Neglecting the second order effects, we can see the shear deformation changes only θ_{M-M-N} , while the orthorhombic deformation changes both L_{M-M} and θ_{M-M-N} . Hence the contributions of the bond angle deviation to the deformation energy are of the same order in both deformation modes under the condition of

$$\gamma/2 = \varepsilon. \quad (12)$$

Using this constraint we can compare the deformation energies of applied orthorhombic and shear strain on the cubic systems (see Fig. 4). These energies are given by parabolic functions as follows:

$$U_{\text{ortho}}/V_0 = \frac{1}{2} c_{11} \left[\varepsilon^2 + \frac{\varepsilon^2}{(1 + \varepsilon)^2} \right] - c_{12} \frac{\varepsilon^2}{1 + \varepsilon} \sim (c_{11} - c_{12}) \varepsilon^2, \quad (13)$$

$$U_{\text{shear}}/V_0 = \frac{1}{2} c_{44} \gamma^2. \quad (14)$$

Since both the deformation modes conserve the unit-cell volume V_0 , the anisotropy coefficient κ can be written as the ratio of these deformation energies:

$$\kappa = U_{\text{ortho}}/U_{\text{shear}}, \quad (15)$$

under the same constraint (12). In Fig. 4, lines indicate the theoretical deformation energy based on the present elastic constants, and symbols indicate the calculated energy from the self-consistent field obtained with $1550 \mathbf{k}$ points by the $18 \times 18 \times 18$ mesh for the shear mode and $4505 \mathbf{k}$ points by the $32 \times 32 \times 32$ mesh for the orthorhombic mode. It is

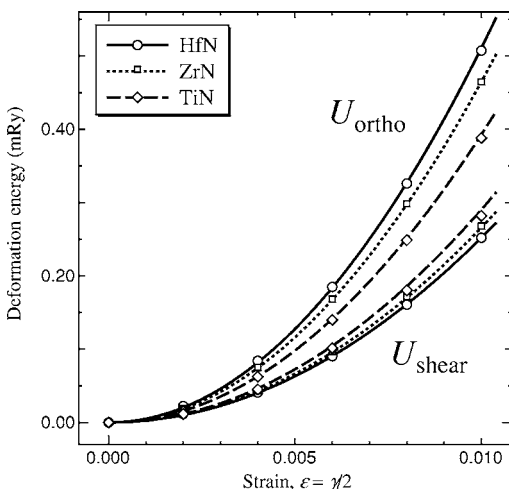


FIG. 4. Deformation energy of HfN, ZrN, and TiN by orthorhombic and shear strain with keeping the unit cell volume. The marks and lines in the figure denote total energy by self-consistent calculation and elastic energy by Hooke's law with the present elastic constants, respectively.

clearly seen that U_{shear} of these three materials are similar to each other, but U_{ortho} is different. Furthermore, the difference between U_{ortho} and U_{shear} which indicates the contribution of $\Delta L_{\text{M-M}}$ is small for TiN ($\kappa=1.36$), but large for HfN ($\kappa=2.02$). This means the high deformation energy of these materials are mainly caused by the resistance of the angle between M-M-N bondings in (100),¹⁰ but the elastic anisotropy itself by the radial atomic distance of metal-nitrogen covalent bond.

IV. CONCLUDING REMARKS

Ab initio calculations of elastic constants in TiN, ZrN, and HfN with systematic verifications of \mathbf{k} -point convergence showed that a much larger set of k points than has been

previously employed, is needed to achieve good convergence in all elastic constants. The good convergence allowed a discussion of the anisotropy of the elastic properties for IVB transition-metal nitrides. The results obtained for these materials exhibit an anisotropy according to the cubic NaCl structure, and agree with the anisotropic lattice distortions detected by XRD. It is surprising that the experimentally observed lattice distortions in thin films can be explained based only on the elastic properties of the system, without modeling of the microstructures in the specimen. Furthermore, the anisotropy coefficient increases with the atomic number of the transition metal element. Due to the strong anisotropy, the Young's modulus of HfN varies from 300 GPa to approximately 600 GPa depending on the crystallographic direction. Hence, it is difficult to determine a single averaged value of the Young's modulus for a bulk polycrystalline specimen.

The discussion of the deformation energy revealed that the anisotropy comes from the covalent metal-nitrogen bonding along $\langle 100 \rangle$, although the high deformation energy is caused by the angular deviation between M-M-N bonding in the (001) plane. This connects the variation of the elastic anisotropy among HfN, ZrN, and TiN to the different quantum numbers of the hybridized covalent bonding.

Overall, the present study encourages obtaining further understanding of the macroscopic elasticity of hard metal nitrides from the intrinsic properties of the atomic and electronic structure in the crystal systems.

ACKNOWLEDGMENTS

We are grateful to K. Heiskanen, A. Kuronen, A. Lehto, and N. Juslin for invaluable discussions. We are thankful for grants of computer time from CSC, Finland. The authors acknowledge financial support by the Academy of Finland through Consortium NAKAMA Research Project No. 210850 (S.N. and R.N.) and through the Centers of Excellence Program 2006-2011 (K.N.).

*Electronic address: shijo.nagao@hut.fi

¹H. O. Pierson, *Handbook of Refractory Carbides and Nitrides* (Noyes Publishing, New Jersey, 1996).
²H. von Seefeld, N. W. Cheung, M. Mäenpää, and M. A. Nicolet, *IEEE Trans. Electron Devices* **27**, 873 (1980).
³C. Y. Ting, *Thin Solid Films* **119**, 11 (1984).
⁴G. Gagnon, *J. Appl. Phys.* **79**, 7612 (1996).
⁵R. Nowak and C. L. Li, *Thin Solid Films* **305**, 297 (1997).
⁶S. Yamanaka, H. Kawaji, K. Hotehama, and M. Ohashi, *Adv. Mater. (Weinheim, Ger.)* **8**, 771 (1996).
⁷S. Yamanaka, K. Hotehama, and H. Kawaji, *Nature (London)* **392**, 580 (1998).
⁸H. Tou, Y. Maniwa, T. Koiwasaki, and S. Yamanaka, *Phys. Rev. Lett.* **86**, 5775 (2001).
⁹A. Zerr, G. Miehe, and R. Riedel, *Nat. Mater.* **2**, 185 (2003).
¹⁰S.-H. Jhi, J. Ihm, S. G. Louie, and M. L. Cohen, *Nature (London)* **399**, 132 (1999).

¹¹Y. Gotoh, M. Y. Liao, H. Tsuji, and J. Ishikawa, *Jpn. J. Appl. Phys., Part 2* **42**, L778 (2003).
¹²R. Nowak and S. Maruno, *Mater. Sci. Eng., A* **202**, 226 (1995).
¹³R. Nowak, Y. Horino, Y. Ando, and S. Maruno, *Appl. Phys. Lett.* **68**, 3743 (1996).
¹⁴R. Nowak, F. Yoshida, Y. Miyagawa, and S. Miyagawa, *Nucl. Instrum. Methods Phys. Res. B* **148**, 232 (1999).
¹⁵R. Nowak, F. Yoshida, J. Morgiel, and B. Major, *J. Appl. Phys.* **85**, 841 (1999).
¹⁶P. Nimmagada and R. F. Bunshah, *Thin Solid Films* **63**, 327 (1979).
¹⁷A. Grill and P. R. Aron, *Thin Solid Films* **108**, 173 (1983).
¹⁸W. D. Sproul, *Thin Solid Films* **119**, 227 (1984).
¹⁹B. O. Johansson, J. E. Sundgren, and U. Helmersson, *J. Appl. Phys.* **58**, 3112 (1985).
²⁰H. A. Jehn, U. Kopacz, and S. Hofmann, *J. Vac. Sci. Technol. A* **3**, 2406 (1985).

- ²¹X.-J. Chen, V. V. Struzhkin, Z. Wu, M. Somayazulu, J. Qian, S. Kung, A. N. Christensen, Y. Zhao, R. E. Cohen, H.-K. Mao *et al.*, Proc. Natl. Acad. Sci. U.S.A. **102**, 3198 (2005).
- ²²R. Nowak, C. L. Li, and S. Maruno, J. Mater. Res. **12**, 64 (1997).
- ²³M. Zhang and J. He, Surf. Coat. Technol. **142-144**, 125 (2001).
- ²⁴S. Fayeulle, A. Misra, H. Kung, and M. Nastasi, Nucl. Instrum. Methods Phys. Res. B **148**, 227 (1999).
- ²⁵G. Abadias and Y. Y. Tse, J. Appl. Phys. **95**, 2414 (2004).
- ²⁶I. Goldfarb, J. Pelleg, and L. Zevin, Thin Solid Films **200**, 117 (1991).
- ²⁷C. Stampfl and C. G. Van de Walle, Phys. Rev. B **59**, 5521 (1999).
- ²⁸A. Zaoui, B. Bouhafs, and P. Ruterana, Mater. Chem. Phys. **91**, 108 (2005).
- ²⁹C. Stampfl, W. Mannstadt, R. Asahi, and A. J. Freeman, Phys. Rev. B **63**, 155106 (2001).
- ³⁰A. J. Perry, Thin Solid Films **193/194**, 463 (1990).
- ³¹J. Tersoff, Phys. Rev. B **37**, 6991 (1988).
- ³²D. W. Brenner, Phys. Rev. B **42**, 9458 (1990).
- ³³K. Albe, K. Nordlund, and R. S. Averback, Phys. Rev. B **65**, 195124 (2002).
- ³⁴J. Nord, K. Albe, P. Erhart, and K. Nordlund, J. Phys.: Condens. Matter **15**, 5649 (2003).
- ³⁵N. Juslin, P. Erhart, P. Träskelin, J. Nord, K. O. E. Henriksson, K. Nordlund, E. Salonen, and K. Albe, J. Appl. Phys. **98**, 123520 (2005).
- ³⁶S. Baroni, S. de Gironcoli, A. D. Corso, and P. Giannozzi, Rev. Mod. Phys. **73**, 515 (2001).
- ³⁷D. Vanderbilt, Phys. Rev. B **41**, 7892 (1990).
- ³⁸O. H. Nielsen and R. M. Martin, Phys. Rev. B **32**, 3780 (1985).
- ³⁹M. Methfessel and A. T. Paxton, Phys. Rev. B **40**, 3616 (1989).
- ⁴⁰H. J. Monkhorst and J. D. Pack, Phys. Rev. B **13**, 5188 (1976).
- ⁴¹J. F. Nye, *Physical Properties of Crystals* (Oxford University Press, Oxford, 1985).